Control mechanisms for the oceanic distribution of silicon isotopes

André G. Wischmeyer,[1] Christina L. De La Rocha,[2] Ernst Maier-Reimer,[3]
and Dieter A. Wolf-Gladrow[1]

[1]   Marine diatoms take up silicic acid for the buildup of their opaline shells and discriminate against the heavier silicon isotope. For the first time, the overall oceanic distribution of silicon isotopes has been estimated by integration of the Hamburg Model of the Ocean Carbon Cycle, version 4 (HAMOCC4). It is shown that the relationship between the silicic acid concentration and its silicon isotope composition is not a simple Rayleigh distillation curve. Only the Southern Ocean and the equatorial Pacific show a clear functional dependency similar to the Rayleigh distillation curve. Model results can be used to predict opal silicon isotope compositions in the sediment and constrain the use of silicon isotopes as a proxy for silicic acid utilization. Owing to the structure of the Pacific current system, it might be valid to apply a relationship between surface silicic acid concentrations and the silicon isotope signal in the equatorial Pacific sediments.   *INDEX TERMS:* 1615 Global Change: Biogeochemical processes (4805); 1635 Global Change: Oceans (4203); 3030 Marine Geology and Geophysics: Micropaleontology; 4870 Oceanography: Biological and Chemical: Stable isotopes; *KEYWORDS:* LGM, silicic acid concentrations, silicic acid utilization, silicon isotopes

1.   Introduction

[2]   Diatoms play an important role in the fixation and export of organic matter from the euphotic zone to the deep ocean. Since diatoms require silicon for growth, there is a steadily growing interest in the study of the marine silica cycle. The accumulation of opal in sediments has often been used as a tracer of productivity, but there is some question as to what degree opal production may be decoupled from opal accumulation in the ocean [*Ragueneau et al.*, 2000]. Reconstruction of the concentration and biological drawdown of silicic acid in the ancient surface ocean would be of great use to the study of primary production and silica cycling in the past. One means of assessing past ocean productivity is through modeling, but modeling biological productivity at the Last Glacial Maximum (LGM) always suffers from the lack of direct measurements.

[3]   Forcing LGM ocean general circulation models (OGCMs) or coupled ocean-atmosphere models has to rely on proxies and results (e.g., biomass production) have to be compared with contradictory proxy results [*Loubere*, 2000; *De La Rocha et al.*, 1998]. It becomes important then to assess the reliability of proxies in the reconstruction of past oceanic and climatic conditions. A long line of proxy data is already available for many important climate variables [*Wefer et al.*, 1999]. Among those are temperature (alkenone unsaturation ratio in coccolithophores or Mg/Ca ratios in foraminifera), sea level ($\delta^{18}O_{ice-cores}$), pH ($\delta^{11}B$ in foraminifera), and nitrate utilization ($\delta^{15}N$ in organic matter), to name just a few. The closer we look at these proxies the more we are aware of their pitfalls [*Wefer et al.*, 1999].

[4]   Recent work taking advantage of the fractionation of silicon isotopes by marine diatoms has suggested that the silicon isotopic composition of diatom opal may be used to reconstruct the cycling of silicon within the surface ocean [*De La Rocha et al.*, 1997, 1998]. To date, however, a critical assessment of silicon isotopes as a proxy of silicic acid utilization has not been carried out. The current work presents results from the Hamburg Model of the Ocean Carbon Cycle, version 4, (HAMOCC4) for the marine distribution of silicon isotopes. It will be investigated whether the use of silicon isotope ratios of diatom frustules is a valid approach to derive past silicic acid utilization. Furthermore, silicon isotope ratios will as well be examined as a potential proxy for absolute silicic acid concentrations.

2.   Silicon Isotopes

[5]   The three stable isotopes of silicon are ^{28}Si, ^{29}Si, and ^{30}Si with abundances of 92.22% ^{28}Si, 4.68% ^{29}Si, and 3.08% ^{30}Si, respectively [*Rosman and Taylor*, 1998]. Isotope ratios for silicon are defined by the abundance of the rare isotope divided by the abundance of the most abundant isotope,

$$^{30}R = \frac{^{30}Si}{^{28}Si}. \tag{1}$$

[1]Alfred Wegener Institute for Polar and Marine Research, Bremerhaven, Germany.
[2]Department of Earth Sciences, University of Cambridge, Cambridge, UK.
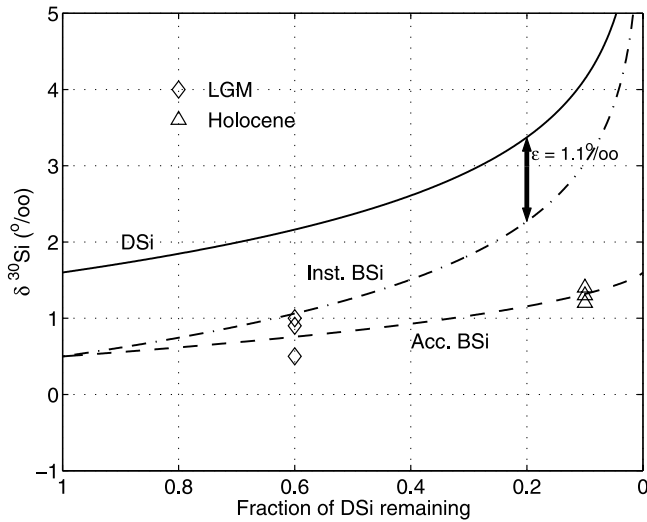[3]Max Planck Institute for Meteorology, Hamburg, Germany.

Figure 1. View graph of the Rayleigh distillation curves under the assumption of a closed system and LGM and Holocene sediment data [*De La Rocha et al.*, 1998].

The fractionation factor α is defined by

$$^{30}\alpha = \frac{^{30}R_A}{^{30}R_B}, \tag{2}$$

where $^{30}R_A$ and $^{30}R_B$ are the isotope ratios of educt A and product B of a process (here: the uptake and fixation of silicic acid in a diatom frustule). Since α is close to 1, the fractionation ϵ, i.e., the deviation of α from 1 in parts per thousand (‰), is commonly used,

$$\epsilon = (\alpha - 1) \cdot 1000 \quad (‰). \tag{3}$$

For instance, for the process of silicic acid fixation by diatoms ϵ is -1.1‰. For silicic acid fixation by sponges, ϵ is about -3‰ [*De La Rocha*, 2003]. The isotopic composition of compounds (equation (6)) is reported as a ratio normalized to some standard value. In the case for silicon the standards are $^{29}R_{\text{NBS-28}}$ and $^{30}R_{\text{NBS-28}}$,

$$^{29}R_{\text{NBS-28}} = \frac{^{29}\text{Si}}{^{28}\text{Si}} = \frac{4.6853\%}{92.22223\%} \tag{4}$$

$$^{30}R_{\text{NBS-28}} = \frac{^{30}\text{Si}}{^{28}\text{Si}} = \frac{3.0924\%}{92.22223\%}, \tag{5}$$

where NBS stands for the United States National Bureau of Standards [*Coplen et al.*, 2002]. Again, since the differences in isotope ratios are generally very small and the ratios R are close to unity, the isotopic signal of a sample A relative to a standard is reported as the deviation δ from one in parts per thousand (‰),

$$\delta^{30}\text{Si} = \left(\frac{^{30}R_{sample}}{^{30}R_{\text{NBS-28}}} - 1 \right) \cdot 1000. \tag{6}$$

Here δ (in ‰) describes the accumulated signal or the overall composition of a sample, whereas the fractionation process is described by α or ϵ (Figure 1).

[6] If elements such as silicon have more than two stable isotopes and the fractionation is mass dependent, the fractionation between one pair of isotopes can be approximated by the fractionation factor of the other pair of isotopes [*Criss*, 1999],

$$^{29}\alpha = {}^{30}\alpha^z \tag{7}$$

where z depends on the isotope masses as follows:

$$z = \frac{30}{29} \cdot \frac{29 - 28}{30 - 28} \approx 0.517. \tag{8}$$

2.1. Fractionation of δ^{30}Si by Diatoms

[7] In a number of laboratory experiments, *De La Rocha et al.* [1997] examined the possible fractionation of silicon isotopes in diatom frustules. Three different species of common laboratory diatoms showed a preference of the lighter isotope ^{28}Si over ^{30}Si with a practically identical fractionation (Table 1). This resulted in a fractionation factor $^{30}\alpha$ of

$$^{30}\alpha = \frac{R_{Opal}}{R_{DSi}} = 0.9989, \tag{9}$$

where R_{Opal} and R_{DSi} are the mole ratios of ^{30}Si to ^{28}Si in opal and silicic acid, respectively. Opaline frustules were about 1.1‰ isotopically lighter (i.e., depleted in ^{30}Si with an $\epsilon = -1.1$) than the silicic acid in the water they were built from. Neither did $^{30}\alpha$ seem to be temperature dependent in the range from 12°C to 22°C, nor was it dependent on the growth rate. The measured fractionation factor was identical to the one found for the species *Phaeodactylum tricornutum* about 20 years ago [*Spadaro*, 1983]. Under the assumption that the silicic acid taken up by diatoms is supplied from a finite pool of Si, continuous uptake of silicic acid progressively changes the isotope signal of both the silicic acid pool and the biogenic opal (Figure 1). This process is called Rayleigh distillation. The isotopic composition of diatom frustules is made up of relatively greater proportions of ^{30}Si as the concentration of silicic acid goes down. Thus the silicon isotopic composition can give information about the fraction of dissolved silicic acid (DSi) taken up and thereby also on the diatom productivity. The Rayleigh distillation theory can be applied to ocean areas under certain conditions in which water parcels are separated from surrounding water masses

Table 1. Silicon Isotope Fractionation During Biogenic Silica Formation for Three Diatom Species Given by *De La Rocha et al.* [1997]

Diatom	α
Skeletonema costatum	0.9990 ± 0.0004
Thalassiosira weissflogii	0.9987 ± 0.0004
Thalassiosira sp.	0.9989 ± 0.0004

(closed system). Since the diatom frustules, as they are buried in the ocean sediments, reflect the signal of surface waters, the analysis of these frustules can give information on the silicon utilization at the time of frustule formation, i.e., also for the geological past.

2.2. Measured Distribution of $\delta^{30}Si$
2.2.1. The $\delta^{30}Si$ in Rivers
[8] The average isotope compositions of silicic acid of river waters measured so far are [*De La Rocha et al.*, 2000]:

$$\delta^{30}Si_{DSi,riv} = 0.8(\text{‰}).$$

The $\delta^{30}Si$ values vary between different locations up to 0.7‰ and within the same river by up to 0.4‰. From the relative abundances of the silicon isotopes on Earth and with the total riverine flux of Si,

$$TSi_{riv} = {}^{28}Si_{riv} + {}^{29}Si_{riv} + {}^{30}Si_{riv}, \qquad (10)$$

the riverine flux of $^{30}Si_{riv}$ can readily be calculated. Together with a TSi_{riv} of 5.6 Tmol silica [*Tréguer et al.*, 1995] the influx of silicon isotopes is

$$^{30}Si_{riv} = 0.17 \text{ Tmol Si yr}^{-1}.$$

2.2.2. The $\delta^{30}Si$ in Seawater
[9] From 69 marine samples of $\delta^{30}Si_{DSi}$ the averaged $\delta^{30}Si$ of the ocean is $+ 1.1 \pm 0.3$‰ with a range from $+0.6$‰ to $+1.7$‰ [*De La Rocha et al.*, 2000]. Most of these data were measured at depths below 200 m since in surface waters with $[H_4SiO_4]$ less than 10 μmol kg^{-1} it is very difficult to measure $\delta^{30}Si$. Surface waters were estimated to have a $\delta^{30}Si$ up to $+3$‰. Below, it will be shown that this is a very low estimate. Generally, surface water or waters at shallow depths seem to be most positive [*De La Rocha et al.*, 2000]. Vertical gradients of $\delta^{30}Si_{DSi}$ suggested $\delta^{30}Si$ minimum values below 1000 m. Values of the deep Pacific seem to be 0.4‰ lighter than values at the corresponding depth in the Atlantic. Given the difficulty of the measurements and the maximum precision of 0.1‰, it is difficult to interpret the vertical gradients in the ocean interior.

2.2.3. The $\delta^{30}Si$ in Sediments
[10] Three sediment cores south of the current Southern Ocean Polar Front show a glacial-interglacial variation in the silicon isotope composition of diatom frustules [*De La Rocha et al.*, 1998]. At the LGM the isotope composition of the frustules was about 0.7‰ lighter than today. This was explained by a 50% reduction of silicic acid utilization at the LGM compared to today (Figure 1). Recently, results from a $\delta^{30}Si$ record over the last 300 ka also suggested less silicon utilization during the last three glacial periods [*Brzezinski et al.*, 2002].

3. A Model for the Global Ocean Silicon Cycle
3.1. HAMOCC4 Model Setup
[11] HAMOCC4 is driven by monthly fields of advection, convection, temperature, and salinity from the Ham-

burg Large Scale Geostrophic ocean circulation model (LSG [*Maier-Reimer et al.*, 1993]). The LSG itself is forced by temperature data from COADS [*Woodruff et al.*, 1987] and wind fields of *Hellerman and Rosenstein* [1983]. Salinity is restored to *Levitus* [1982] data. Sea ice coverage is taken from the dynamical sea ice model of LSG. The underlying grid is a 3.5° by 3.5° Arakawa E-grid [*Arakawa and Lamb*, 1977] with 15 vertical layers down to the realistic (but smoothed) bottom topography. Tracers are advected with the help of an upstream scheme. For this study we focused on silicon. Other tracers are only mentioned if they are directly related to the Si cycle.

[12] Of particular interest to this study are the Southern Ocean and the equatorial Pacific. As it is well known for general circulation models, also the HAMOCC4 does not perfectly reproduce mixing in the Southern Ocean. This is also due to the missing representation of mesoscale eddies. One indication for the proper reconstruction of the Southern Ocean overturning is the Ekman transport along the Antarctic Circumpolar Current that has been estimated by local inverse modeling to 34 Sv [*Sloyan and Rintoul*, 2001]. The HAMOCC4 model gives a corresponding transport of 27 Sv, which is a good result for a model with a comparatively coarse grid. Similarly, the strength of the equatorial Pacific upwelling in the model (52 Sv) is close to estimated values and therefore an indication of a sufficient representation of the model physics in the areas of interest (see below). Furthermore, the model was also tested for distributions of CFCs and radiocarbon in the Southern Ocean and compares well with other general circulation models [*Dutay et al.*, 2002].

[13] Monthly velocity fields are interpolated to ten 3-day time slices to allow for a sufficiently short integration time of the biological module. Each biologically active element fulfills the tracer equation,

$$\frac{\partial C_i}{\partial t} = -\nabla \vec{U} C_i - D C_i + \Theta_i(C_i) + F_i(C_i, C_j), \qquad (11)$$

where C_i denotes tracers, $\vec{U}$ is the advection velocity, D is the diffusion operator, Θ represents tracer specific source and sink terms (e.g., riverine input of silicon isotopes) and F_i is the nonlinear (biologically mediated) interaction between the different tracers.

[14] The biomass limiting nutrient is phosphate (PO_4^{3-}), which is consumed by phytoplankton. Phytoplankton uptake of PO_4^{3-} is described by

$$\frac{\partial PO_4^{3-}}{\partial t} = \mu \cdot Phyto \cdot \frac{PO_4^{3-}}{PO_4^{3-} + k_{PO_4^{3-}}}, \qquad (12)$$

with the growth rate μ depending on temperature T (°C) and light L (W m^{-2}) (see below and Table 2 for model parameters). Sources of PO_4^{3-} in the water column include bacterial remineralization of dissolved organic and particulate organic material, and remineralization of inefficiently grazed and left over phytoplankton (see *Six and Maier-Reimer* [1996] for details).

Table 2. Parameters Used by the Biological Module of HAMOCC4

Definition	Value
Grazer assimilation efficiency: z_{inges}	0.5
Maximum grazing rate: ω	0.8 d^{-1}
Phosphate half saturation conc.: $k_{PO_4}^{3-}$	0.04 $\mu mol\ P\ L^{-1}$
Grazing half saturation conc.: $Grazer_0$	4 $\mu mol\ C\ L^{-1}$
Grazer mortality: γ_{Gra}	0.06 d^{-1}
Phyto. mortality: γ_{Phy}	0.008 d^{-1}
Minimum Grazer conc.: $Grazer_{min}$	0.001 $\mu mol\ C\ L^{-1}$
Minimum Phyto. conc.: $Phyto_{min}$	0.001 $\mu mol\ C\ L^{-1}$
Photosynthetically active radiation: PAR	0.4
Initial slope of the P-I curve: α	0.03 $d^{-1}\ m^2\ W^{-1}$
Light extinction coefficient: k	0.025 m^{-1}
Growth rate at 0°C: a	0.8 d^{-1}
Temperature sensitivity of growth: b	1.066
Temperature dependence of growth: c	1 K^{-1}

[15] The equation for phytoplankton reads

$$\frac{\partial Phyto}{\partial t} = Phyto \cdot \mu \cdot \frac{PO_4^{3-}}{PO_4^{3-} + k_{PO_4^{3-}}} - \omega \cdot Grazer$$
$$\cdot \frac{Phyto - Phyto_{min}}{Phyto + Grazer_0} - (Phyto - Phyto_{min}) \cdot \gamma_{Phy}. \quad (13)$$

The growth rate μ depends on temperature and light [*Smith*, 1936],

$$\mu = \frac{f(T) \cdot g(L)}{\sqrt{f(T)^2 \cdot g(L)^2}}$$

$$\text{with } f(T) = a \cdot b^{cT} \quad \text{(after Eppley, 1972)}$$

$$\text{and} \quad g(L) = I_0 \alpha PAR \frac{1}{z} \int e^{-kz} dz,$$

where I_0 is the surface irradiance in $W\ m^{-2}$, PAR describes the amount of photosynthetically active radiation, α is the initial slope of the P-I curve, and k is the light extinction coefficient.

[16] The change of grazers is described by

$$\frac{\partial Grazer}{\partial t} = Grazer \cdot \omega \cdot z_{inges} \cdot \frac{Phyto - Phyto_{min}}{Phyto + Grazer_0}$$
$$- \gamma_{Gra}(Grazer - Grazer_{min}). \quad (14)$$

The differentiation between buildup of biogenic opal or calcite is carried out similar to *Maier-Reimer* [1993]. There is a smooth transition from opal production (P(opal)) by diatoms under silicic acid replete conditions to calcite production P(calcite) by coccolithophores when silicic acid is depleted,

$$P(opal) = \min\left(60 \cdot \Delta PO_4^{3-}, \frac{H_4 SiO_4 \cdot \Delta PO_4^{3-}}{PO_4^{3-} + \Delta PO_4^{3-}}\right)$$

$$P(calcite) = 0.5\left(\frac{0.5\Delta PO_4^{3-} - \frac{P(opal)}{122}}{\Delta PO_4^{3-}}\right) \quad (15)$$

$$\text{with } \Delta PO_4^{3-} = \mu \cdot Phyto \frac{PO_4^{3-}}{PO_4^{3-} + PO_{4,0}^{3-}} \Delta t.$$

This formulation ensures that at any location the rain ratio "Calcite:Organic Carbon" ranges from 0.05 to a maximum of 0.25. Global average of the rain ratio of particle export, i.e., particles that leave the top 100 m, is approximately 0.2.

[17] Particulate matter that sinks out of the euphotic zone is transported to depth with a sinking speed of 5 m d^{-1}. Opal dissolves with a temperature dependent dissolution rate of $l(month^{-1}) = 0.01(K^{-1}\ month^{-1}) \cdot (T(°C) + 2°C)$. Temperature-dependent dissolution of opal has been described by, for example, *Kamatami and Riley* [1979] and *Tréguer et al.* [1989]. The factor 0.01 is chosen to fit the global average vertical silicic acid concentration gradient. A slightly modified version of the sophisticated sediment model by *Heinze et al.* [1999], now with an implicit iteration scheme is used to describe accumulation, dissolution, and burial of particulate matter. Riverine input balances the matter that leaves the lowest sediment layer. The silicic acid saturation concentration in the pore water of the sediment is set to a global average of 820 $\mu mol\ Si\ L^{-1}$, which is slightly below the maximum value of 900 $\mu mol\ Si\ L^{-1}$ measured in sediment porewaters [*Ragueneau et al.*, 2000]. Our global average might be too high, but since the redissolution of opal from the sediments and the accumulation of opal on the sediment is similar to what has been estimated before, we stay with this value. We are aware of the fact that it will be necessary to include a spatially varying silicic acid saturation concentration in future model versions.

3.2. Spinup

[18] The model that was used for this study already had a compartment for total Si. To allow calculation of $\delta^{30}Si$, silicon 30 was added. Owing to the small magnitude of the fractionation of silicon isotopes by diatoms and in order to precisely calculate $\delta^{30}Si$ the number of iterations of the implicit temporal tracer integration had to be increased compared to other HAMOCC4 runs. This increased the computation time by a factor of 2 (100 model years $\simeq 10^4$ CPU seconds on a NEC SX6 computer).

[19] Starting with a distribution of tracers given by HAMOCC3.1 [*Six and Maier-Reimer*, 1996], the model was run for 23,000 model years into a new close to equilibrium state (atmospheric CO_2 of 280 ppmv). The turnover time for silicon in the ocean is about 16,000 years [*Tréguer et al.*, 1995]. The silicon isotope composition of the water was initialized with the modern river silicon isotope composition. River runoff is equally distributed around the continental margins. This simplification of the real situation is assumed to have a comparatively small effect on the model results, because the turnover time of silicon in the ocean is about an order of magnitude faster than the mixing time of the ocean.

[20] The total amount of ^{28}Si in the ocean does not change with time because the riverine input is exactly balanced by the burial in the sediments. A steady state in the distribution of the ^{28}Si in silicic acid and biogenic silica is reached after several turnovers of the conveyor belt, i.e., in a few thousand years. On the other hand, the total amount of ^{30}Si in the ocean changes with time. To balance between riverine input of ^{30}Si (in the form of silicic acid) and the
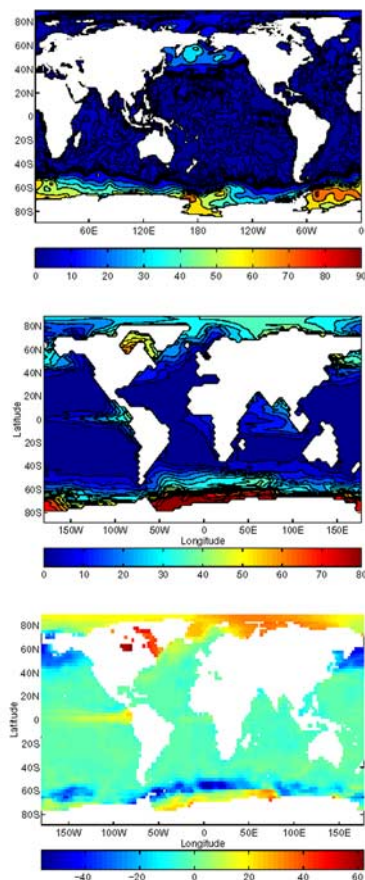
Figure 2. (top) Surface silicic acid concentrations (μmol L^{-1}) as given by the World Ocean Atlas 1998 [*Conkright et al.*, 1998]. (middle) Modeled silicic acid concentrations (μmol L^{-1}) in the top 100 m. (bottom) Silicic acid (μmol L^{-1}): model minus World Ocean Atlas (1998) data. White spaces are land points of either the model or the field data.

burial of ^{30}Si (in the form of biogenic opal) is a self-regulating process. The steady state is approached in time in an exponential way with a time constant of the order of the mean residence time of silicic acid (16 kyr). Thus it takes several times the mean residence time to reach steady state for ^{30}Si, i.e. up to 100,000 years.

[21] A fit of the form

$$\delta^{30}\text{Si} = a(1) - \frac{a(2)}{e^{t/a(3)}}$$

gives an asymptotic value of 1.36‰ for time t $\rightarrow \infty$.

[22] Differences of measured and modeled surface silicic acid concentrations are small in low and mid-latitude areas as well as in the North Atlantic (Figure 2). Two high-nutrient low-chlorophyll areas show larger discrepancies between model results and observations. The North Pacific as well as the Southern Ocean has been found to be iron limited [*Martin and Fitzwater*, 1988; *Boyd et al.*, 2000]. HAMOCC4 uses its dust field only to increase accumula-

tion of particles, i.e., not as an additional iron input that could increase phytoplankton growth rates. Hence the biological production in the Southern Ocean and in the North Pacific draws too many nutrients out of the surface, and thus surface nutrient concentrations are too low.

[23] The far eastern equatorial Pacific seems to have higher than measured silicic acid concentrations. On the one side, this might be due to the coarse model grid and a relatively high vertical diffusivity; on the other side the routines used for the interpolation of the observed silicic acid distribution (Figure 2) tend to flatten out meridional structures. Thus, the high silicic acid tongue along the equator might be underrepresented in the observational, but still gridded and interpolated data. Further differences in the very high northern latitudes including the Hudson Bay are in areas that are often covered by ice. Model processes below northern ice covers are not well known, and hence their model representation (e.g., no phytoplankton growth below ice) might not represent reality. These areas are neglected in further examination. They do not significantly affect the distribution of silicon isotopes in the rest of the oceans.

[24] The pattern of annual opal production in the model in the surface layer agrees well with observations (Figure 3); the model shows highs in areas that are known for high diatom productivity. Maximum values are found in the upwelling areas of the equatorial Pacific, in the Southern Ocean, the northwest Pacific, and the northwest Atlantic.

[25] Gross production of biogenic silica in the Southern Ocean at 170°W between 55°S and 65.5°S has recently been characterized by a pronounced southward increase with a range from 0.76 mol Si m^{-2} yr^{-1} to 3.0 mol Si m^{-2} yr^{-1} [*Nelson et al.*, 2002]. This increase is also found in the model with a mean annual opal production range from 1.1 mol Si m^{-2} yr^{-1} (north) to 3.3 mol Si m^{-2} yr^{-1} (south). In the Indian sector of the Southern Ocean, field observations range from 1.6 to 3.3 mol Si m^{-2} yr^{-1} [*Pondaven et al.*, 2000] with model results between 0.9 mol Si m^{-2} yr^{-1} and 4.5 mol Si m^{-2} yr^{-1}.

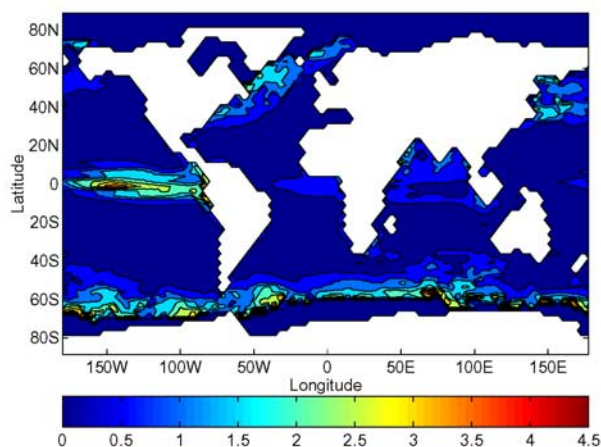**Figure 3.** Annual mean opal production (mol Si m^{-2} yr^{-1}). In the Southern Ocean the edge of the winter ice cover produces a cutoff of the positive values.

[26] Opal that leaves the model euphotic zone and crosses the 100 m depth level, contributes to the opal export production. The model annual average opal export is 177 Tmol Si a^{-1}, which lies perfectly in the range of 240 Tmol Si yr^{-1} for the surface layer production and 120 Tmol Si a^{-1} that crosses the 200 m depth level [*Tréguer et al.*, 1995].

[27] Thirty percent of the exported biogenic material is deposited on the sediment surface, where most of it faces dissolution. About 3% of the deposited material is buried in the sediment and thus closes the model silicon balance. Since dissolution of opal frustules does not seem to alter their isotope composition [*De La Rocha et al.*, 1998], the same dissolution rate was applied to all silicon isotopes in the water column. Silicon compartments in the sediment are treated the same way.

[28] Currently, measurements of silicon isotopes of diatom frustules need on the order of $10^5 - 10^6$ single frustules. Thus the measured signal is an average value of all frustules that accumulated during an earlier bloom event. This fits to the current representation of the buildup and export of opal in the model, where monthly averages (in a $3.5° \times 3.5°$ box) are used despite the time step of 3 days for the biology. If it would be possible to measure the isotope signal in a single frustule, the representation of the accumulation and transport of opal in the model would have to be refined. Then one had to differentiate between opal built at relatively low $\delta^{30}Si_{DSi}$ at the beginning of the month and opal built at relatively high $\delta^{30}Si_{DSi}$ at the end of a month.

4. Modeled Distribution of $\delta^{30}Si$

4.1. The $\delta^{30}Si$ in the Surface Ocean

[29] Comparing the annually averaged surface patterns of $\delta^{30}Si_{DSi}$ with the silicic acid distribution, these two patterns seem to be inversely related (Figures 2 and 4). Low silicic acid concentrations correspond to high $\delta^{30}Si_{DSi}$ values and vice versa. A zero-order explanation for this is as follows: Deep mixing in the high latitudes and equatorial upwelling regions provides high silicic acid concentrations to the euphotic layer; with a zonal average the ultimate sinks of silicic acid would be located in the subtropics such that silicic acid would flow from the high latitudes and the equator to the subtropics. Opal production draws down silicic acid during DSi transport to these endpoints. Hence the subtropical gyres show lowest Si concentrations and highest $\delta^{30}Si$.

[30] However, plotting the two variables against each other (Figure 5) results in a more complicated pattern. Drawing a line through the upper limits of the points (Figure 5) results in a curve similar to the Rayleigh distillation curve (Figure 1), whereas the lower limit is set by the deep ocean average. Plots for the different oceans give similar results (Pacific, Atlantic, and Indian Oceans in Figure 5). All the data between the two wrapping lines are explained by mixing of different water masses.

[31] On a regional scale the surface ocean can show a more closed system Rayleigh behavior. In the equatorial Pacific, water upwells into the euphotic layer where silicifying phytoplankton draws down silicic acid (and other
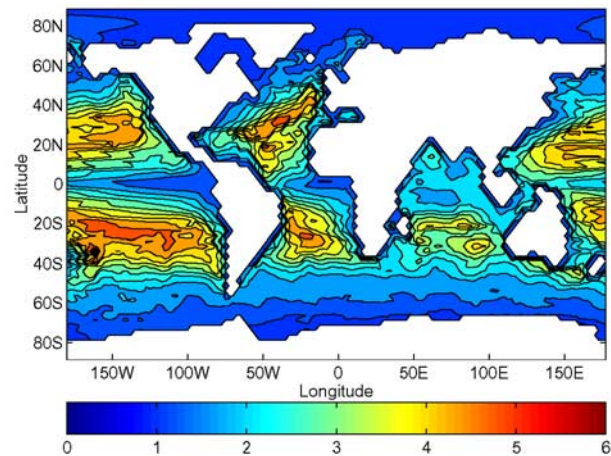

Figure 4. The $\delta^{30}Si$ (‰) of silicic acid in the top 100 m.

nutrients). Consequently, $\delta^{30}Si$ rises (Figure 6, top panel). With the westward transport of water in the South Equatorial Current, opal production further reduces [H_4SiO_4] and the $\delta^{30}Si_{DSi}$ becomes steadily heavier.

[32] The Southern Ocean (Figure 6, bottom panel) shows a similar relationship but with more scatter. Values of $\delta^{30}Si_{DSi}$ above 2‰ reflect ranges of silicic acid of about 10 μmol L^{-1}. This supports the line of arguments drawn by *De La Rocha et al.* [1998], who assumed a closed system type behavior for the silicic acid south of the Antarctic Polar Front. Under this assumption, they could use the Rayleigh distillation curve to get a handle on the relative utilization of silicic acid. With the model $\delta^{30}Si_{DSi}$ of the upwelled water it is now possible to redraw the Rayleigh distillation curve including the sediment signals found by *De La Rocha et al.* [1998]. This will be done below in the section on the signal of $\delta^{30}Si_{opal}$ in the sediment. The data in the lower left corners of Figure 6 are values close to the continental margins and are influenced by river runoff.

[33] Following a single water parcel, especially during the occurrence of a diatom bloom, one would also expect to find Rayleigh-like behaviour throughout the different ocean basins. Unfortunately, there is only very little published $\delta^{30}Si$ data of the silicic acid in the surface ocean available [*De La Rocha et al.*, 2000]. Therefore we cannot compare the model results with measurement. However, it is known that at least in the Southern Ocean, $\delta^{30}Si_{DSi}$ increases as silicic acid concentrations drop moving northward across the Polar Front [*Varela et al.*, 2002].

[34] Whereas the $\delta^{30}Si_{DSi}$ distribution can basically be understood from the simple explanation given above, the picture of $\delta^{30}Si_{opal}$ in the surface layer is more complicated (Figure 7).

[35] High values of $\delta^{30}Si_{opal}$ are also found in the vicinity of the subtropical gyres, but the location of the maximum is shifted toward the equator. Interestingly, additional relative minima can be found at moderate latitudes in an area where one would expect high values; that is, the simple picture drawn above has to be modified. Since the Pacific is much larger than the Atlantic and the subtropical gyres are remote
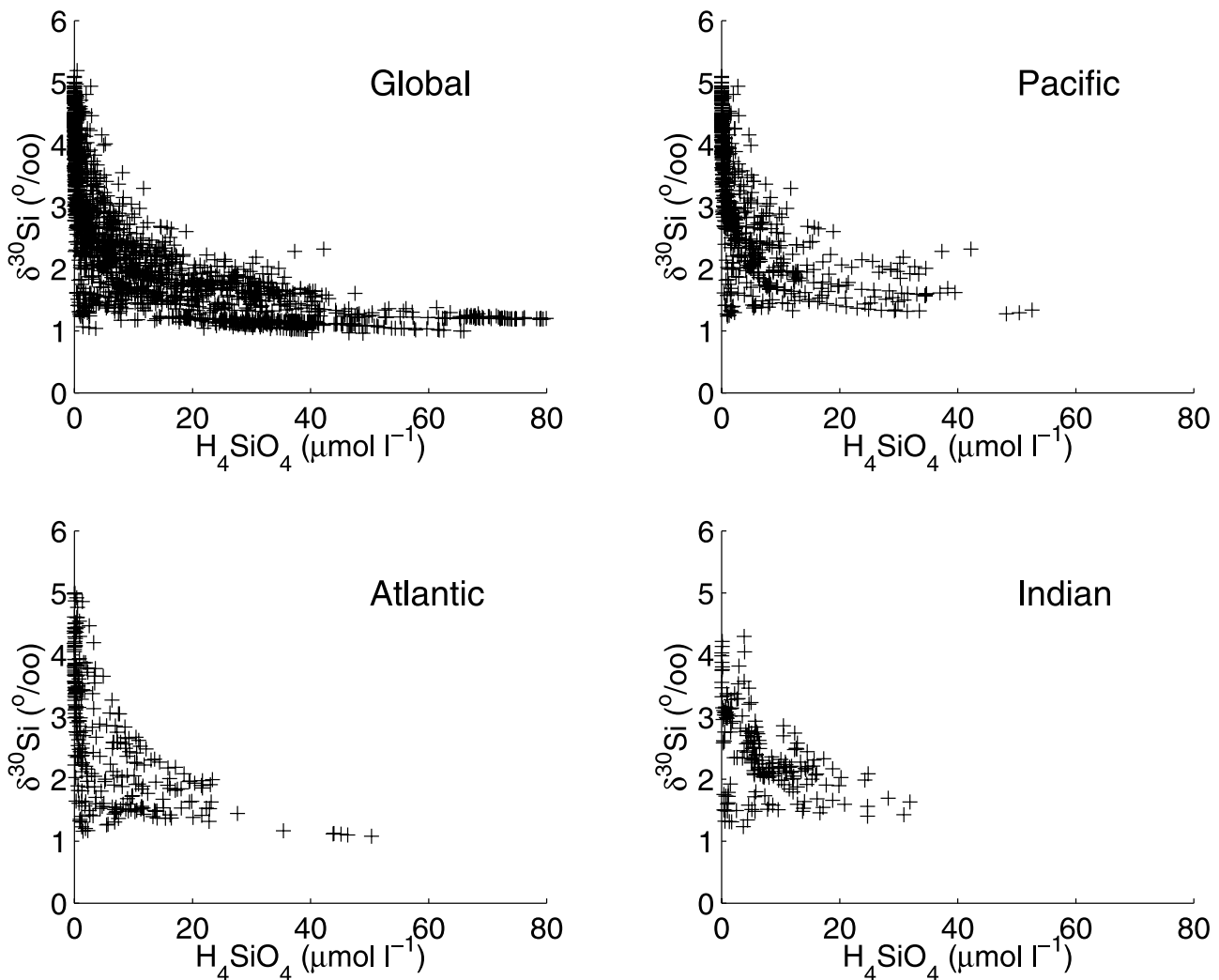
Figure 5. The δ^{30}Si in different ocean basins as a function of H_4SiO_4 concentration, both in the mixed layer.

from strong currents, the broad maxima of δ^{30}Si in the dissolved silica can still be seen in the Pacific δ^{30}Si$_{opal}$ distribution. In the less wide Atlantic, patterns of δ^{30}Si$_{DSi}$ deviate more from the δ^{30}Si$_{DSi}$ distribution because of advection. The accumulation of opal in the surface layer and the rate of production are the keys to understand the δ^{30}Si$_{opal}$ signal. The δ^{30}Si$_{DSi}$ pattern is zonally rather uniform but shows strong meridional gradients; therefore, zonal averages of δ^{30}Si of dissolved silica and opal simplify the diverse patterns and are plotted as a function of time (Figure 8).

[36] The relative minima in the zonally averaged opal δ^{30}Si are located at about 30°N and 30°S. Lowest production rates are found in the area of the opal δ^{30}Si minima between 10°S–40°S and 10°N–40°N. These are the areas with lowest silicic acid concentrations. For the line of arguments we now focus on the Southern Hemisphere at 40°S and 50°S, but the same reasoning holds true for the Northern Hemisphere as well. In spring, diatoms start to grow at 40°S and 50°S in water masses that have very

different silicic acid concentrations, but the isotopic compositions after the winter mixing differ by only a few tenths of a permil. As production draws down silicic acid, δ^{30}Si increases in both the dissolved and the opal phase. Since a part of the diatom biomass remains in the surface water, its opal signal is mixed with that of the following month (Figure 9). Farther south, there is still enough silicon to supply production, but at 40°S, most of the silicon is already taken out and production strongly decreases. Thus comparatively little of the very high δ^{30}Si$_{DSi}$ signal is transferred into the opal and then mixed with the opal signal of the previous month.

[37] At 50°S, production continues and much more opal with a less heavy signal (compared to the north) is built. Production is high, so that the overall δ^{30}Si$_{opal}$ is heavier than 10° farther north. Farther toward the equator the amplitude of the seasonal signal gets smaller, which leads to a more continuous drawdown and less variation in the δ^{30}Si$_{DSi}$ and δ^{30}Si$_{opal}$. South of 50°S the silicic acid concentration is too high to be stronger depleted than at

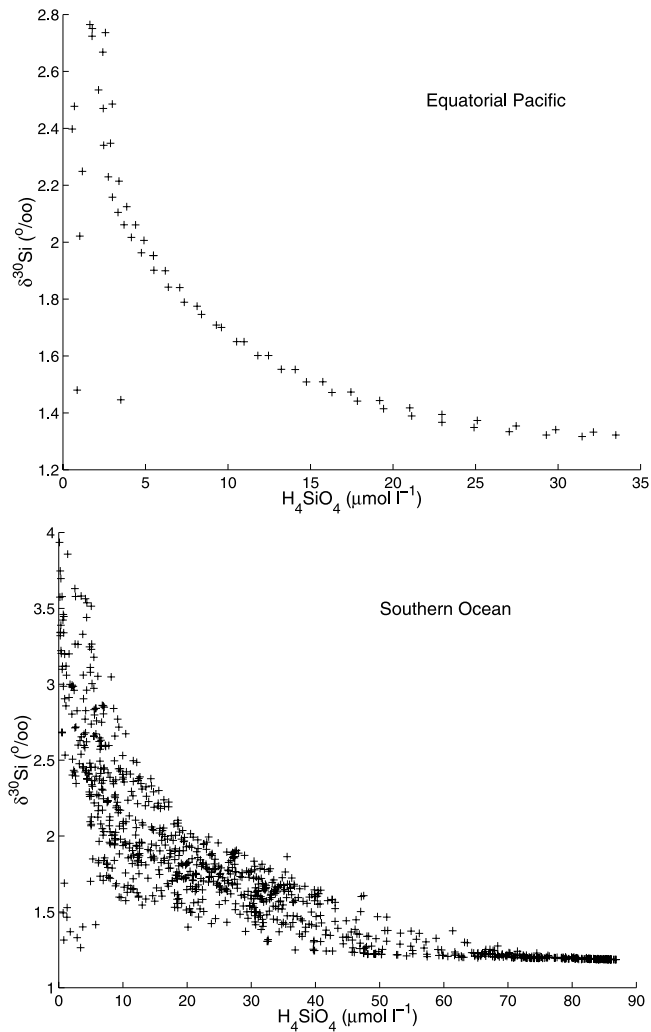**Figure 6.** (top) The δ^{30}Si as a function of H_4SiO_4 concentration in the equatorial Pacific. (bottom) The δ^{30}Si as a function of H_4SiO_4 concentration in the Southern Ocean.
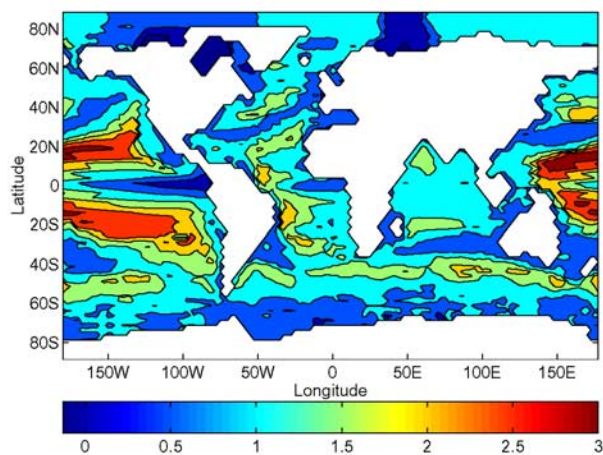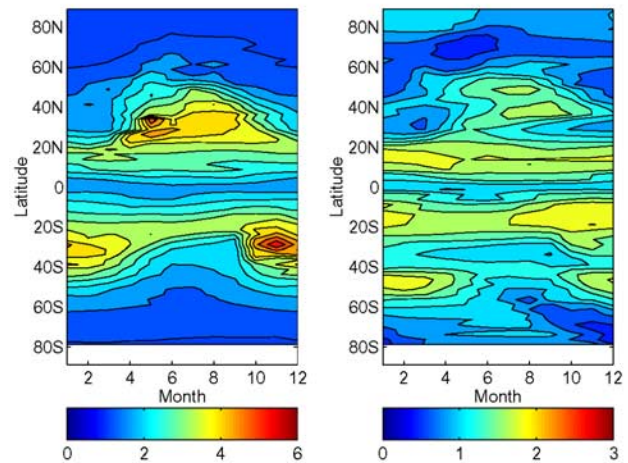

Figure 8. Seasonal cycle of zonal averages of (left) silicic acid δ^{30}Si and (right) oal δ^{30}Si.

50°S. Here δ^{30}Si$_{DSi}$ and δ^{30}Si$_{opal}$ remain comparatively low.

4.2. The δ^{30}Si in the Water Column

[38] The opal isotope signal is transported into the ocean interior, where 97% of the exported opal frustules dissolve. Deep ocean currents are slow relative to surface currents and so the transport of biogenic opal is mainly vertical (not shown here). However, in areas with stronger deep ocean currents, vertically transported opal is mixed with the opal of nearby areas (e.g., at 60°S in the Atlantic Ocean or at
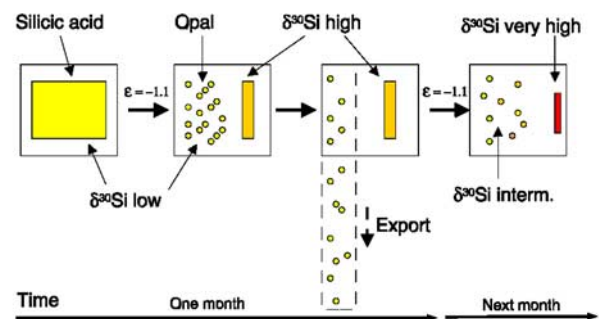

Figure 9. View graph of the temporal development of the δ^{30}Si$_{DSi}$ and δ^{30}Si$_{opal}$ in the model. At the beginning of a productivity event, silicic acid and the opal built from it are low in ^{30}Si (opal is lighter than the silica by 1.1‰, which is not indicated in this simple scheme). After the production, the remaining silicic acid has a higher δ^{30}Si than the opal that is vertically distributed. At the next step in time, production is lower and only little opal with a high δ^{30}Si is built. This new opal mixes with the remaining opal of the month before, which leads to an intermediate signal. Finally, the opal with the intermediate signal is also vertically distributed (not shown).
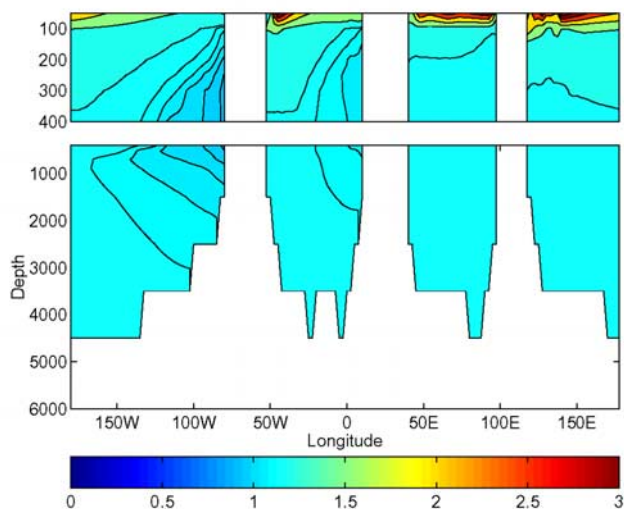

Figure 7. The δ^{30}Si of opal in the ocean surface layer.

Figure 10. The δ^{30}Si of silicic acid along the equator. Contour lines in the deep ocean are every 0.05‰.

about 50°S in the Pacific Ocean). In this version of HAMOCC4, the speed at which opal sinks toward the sediment is 5 m d^{-1}. This value is globally applied and underestimates the sinking speed of opal aggregates formed during blooms. As model opal sinks rather slowly, stronger ocean advection is able to slightly advect the opal isotope signal in the deep ocean. Compared to the amount of silicic acid entering the deep ocean by the vertical pathway, the amount of deep ocean Si is very high; hence vertical gradients in the silicon isotope ratio of the deep ocean are generally small (Figure 10).

[39] Vertical gradients in the top 400 m are more pronounced. Two reasons exist for this. The main reason is that high surface δ^{30}Si of opal influences the upper ocean by temperature dependent dissolution of opal. Second, high vertical diffusivity flattens the sharp gradient between the mixed layer and the underlaying layer in such a way that it
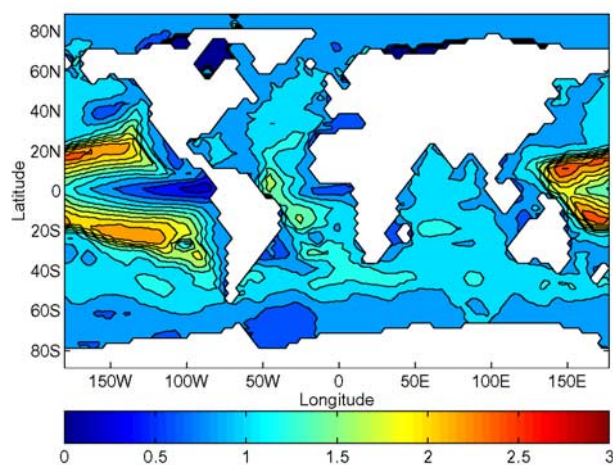

Figure 11. The δ^{30}Si$_{opal}$ at the sediment surface.

Table 3. Comparison of Measured (Core Top) and Modeled ^{30}Si$_{opal}$ for Three Locations, Atlantic Ocean (0°W, 52°S), Indian Ocean I (53°E, 54°W), Indian Ocean II (104°E, 55°S)

3–5 Location	Field	Model		
		Sediment	Surface Average	Surface Range
Atlantic	1.2	1.1	1.2	0.7–1.8
Indian I	1.3	0.9	1.0	0.6–1.4
Indian II	1.4	1.1	1.2	0.5–1.5

is also visible in the upper ocean layers down to about 200 m. Slightly higher δ^{30}Si values of the dissolved phase in the upper ocean have also been found in field data at different locations [*De La Rocha et al.*, 2000]. Except for one profile with strong gradients that were not found at the same location in a later year, the deep ocean results of the model and the field measurements seem to back up. The maximum difference of 0.3‰ is between 500 m and 1000 m below the equatorial upwelling area. The δ^{30}Si$_{DSi}$ minimum below the equatorial Pacific extends from 40°S to 40°N and from the western American coast to about 180°W between 500 m and 3000 m. Similarly, a not as pronounced minimum is found below the Atlantic equatorial upwelling and between the African coast and 30°W in the same depth range. Since the differences in the modeled δ^{30}Si$_{DSi}$ of the rest of the deep ocean are very small (<0.01‰), it will be difficult to compare the model data with measurements that have not yet such a high precision. Still, further data for a better constraint on the deep ocean signal are needed. Plans for the incorporation of δ^{30}Si$_{DSi}$ measurements into the next generation of GEOSECS (GEOTRACER) are under discussion.

4.3. The δ^{30}Si in the Sediment

[40] Dissolution seems to not alter the silicon isotope ratio of opal [*De La Rocha et al.*, 1998]. Therefore the pattern of δ^{30}Si$_{opal}$ in the sediment should mirror the surface opal isotope ratios if export of opal frustules out of the surface was only vertical. Owing to the slow sinking speed of opal, gradients of sediment δ^{30}Si$_{opal}$ are less sharp and maximum values are slightly lower than in the surface layer (Figures 11 and 7).

[41] The δ^{30}Si$_{opal}$ surface pattern of the sediments of the Atlantic Ocean is much more diverse than the one of the Pacific. Areas with the strongest isotope signal in the sediment are areas with the lowest opal percentage. The δ^{30}Si$_{opal}$ in the Atlantic section spans a range of about 1‰, and in the Pacific of about 1.5‰. The δ^{30}Si$_{opal}$ distributions in the Atlantic open ocean sediments are assumed to show a broad scatter that cannot be related easily to surface processes.

[42] Only three sediment cores from the Atlantic and Indian Oceans with δ^{30}Si$_{opal}$ data exist. Measurements of coretop δ^{30}Si$_{opal}$ were slightly higher by 0.1–0.4‰ than the corresponding model results (Table 3).

5. Discussion

5.1. Silicic Acid Utilization in the Southern Ocean

[43] In the Southern Ocean, the difference in silicic acid utilization between the LGM and today was estimated to be
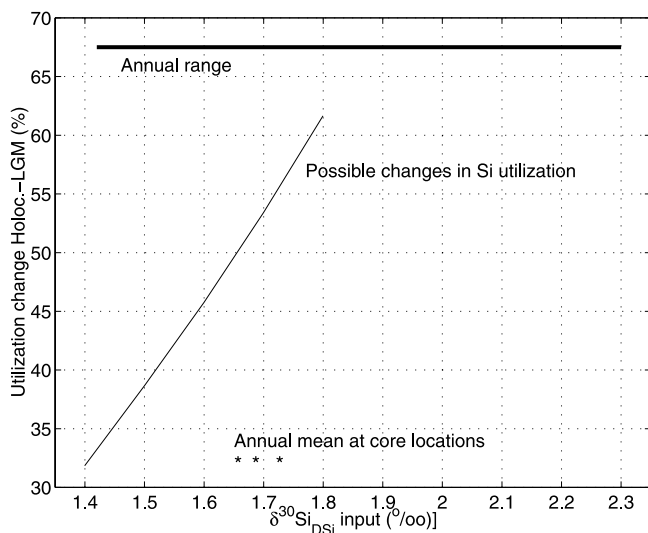
Figure 12. Changes in relative silicic acid utilization as a function of input $\delta^{30}Si_{DSi}$. Also given are the annual range and the annual mean of the model $\delta^{30}Si_{DSi}$ t the three core locations (compare Table 3).

about 50% [*De La Rocha et al.*, 1998]. This is the result of fitting the measured sediment data to the Rayleigh distillation curve for the accumulated biogenic opal. Implicitly included in this is an assumption on the $\delta^{30}Si_{DSi}$ input to the system, which in this case was 1.6‰ (Figure 1). Changing the isotope signal of the input results in changes of the relative utilization (Figure 12). These changes can be quite large, given the slope of the curve for the accumulated matter in Figure 1. If the silicic acid input was upwelled from the deep ocean and thus carries the overall isotopic signature of the ocean interior (in model equilibrium $\delta^{30}Si_{DSi}$ = 1.36‰), the estimated change in silicic acid usage would be below 30%. However, this is not the input signal of the model at the core locations.

[44] In the Indian and Atlantic Oceans at the three locations of the sediment cores used by *De La Rocha et al.* [1998] the modeled $\delta^{30}Si_{DSi}$ varies significantly over the course of the year. The total annual range for the three locations is 1.4–2.3‰, thus spanning a large range of possible changes of the silicic acid utilization. The actual input at the time of highest productivity at the beginning of Southern Hemisphere summer will be at the lower end of the scale. Interestingly again, taking the annual mean of $\delta^{30}Si_{DSi}$ as a first-order approximation to the input at the core locations results in a silicic acid utilization close to the given 50%, which gives support to the conclusions drawn. Since highest silicic acid drawdown takes place before $\delta^{30}Si_{DSi}$ reaches maximum values, the input would be closer to the assumptions of *De La Rocha et al.* [1998]. Even a maximum correction of 0.18‰ due to the still changing deep ocean mean would not change this result (see below).

[45] Sediment data (model $\delta^{30}Si_{opal}$) are lower than the coretop measurements (Table 3), possibly due to the limitations of the opal export scheme. With an opal export scheme that would better represent high export events of

opal, also those data would fit better. All together, model data combined with field measurements give confidence in the use of silicon isotopes as an indicator of silicic acid utilization. If overall opal production in the Southern Ocean at the LGM was reduced, the annual average of $\delta^{30}Si_{DSi}$ might have been lower. A lower $\delta^{30}Si_{opal}$ in the sediment would then mirror higher utilization. Such a change would reduce the estimated utilization change and cannot be ruled out from the model results.

5.2. Surface Ocean Silicic Acid Concentrations in the Equatorial Pacific

[46] At least in the Southern Ocean and in the equatorial Pacific, there is a relationship between the $\delta^{30}Si_{DSi}$ and the silicic acid concentration in the surface (Figure 6). The question now is if this relationship can also be found for the sediment $\delta^{30}Si_{opal}$ and the surface silicic acid concentration. South of 50°S, there is no useful relation between the two quantities (not shown here). Even high $\delta^{30}Si_{DSi}$ values correspond to a range of about 20 μmol Si L^{-1} in the silicate. If at all, only between 50°S and 60°S might a relationship be found. These results are not contradictory to the conclusions drawn by *De La Rocha et al.* [1998] since they relate the relative utilization and not the silicic acid concentrations with the sediment signal.

[47] Results for the equatorial Pacific display an almost perfect relationship between the $\delta^{30}Si_{opal}$ and the silicic acid concentration of the surface water (Figure 13). So far, there is not yet any field data to check the model outcome. It would be of interest to compare the silicic acid concentrations in the equatorial Pacific surface water with the coretop silicon isotope signal along the equator in the Pacific. As long as the structure of the equatorial Pacific current system has been similar in the past, the discovered relationship should be valid, i.e., on glacial-interglacial
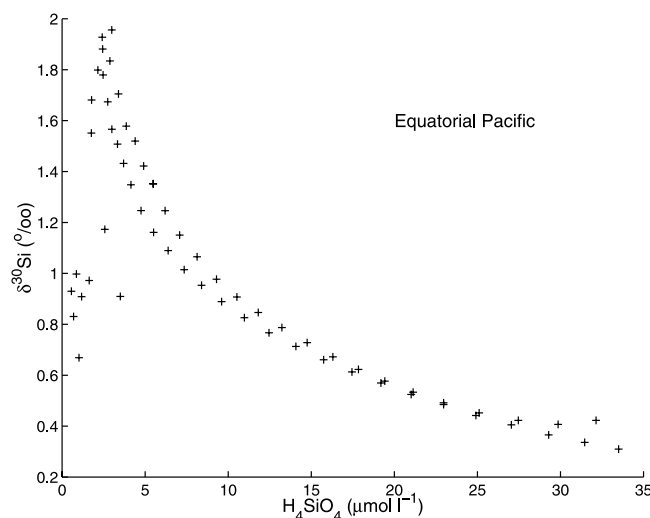

Figure 13. Model data of mean surface silicic acid concentrations (μmol L^{-1}) versus $\delta^{30}Si_{opal}$ in sediment along the equatorial Pacific (2.5°S–2.5°N). The data in the lower left corner are values close to the continental margins and thus influenced by river runoff.

timescales. Given that the downcore signal is dominated by diatoms, silicon isotopes may give important information not only on the relative silicic acid utilization but also on the absolute silicic acid concentration. This is not yet known from any other proxy.

[48] Modeling the global biogeochemical cycle is always constrained by the complexity of the physical and biogeochemical processes that shall be represented and by the amount of computational power that is available. For this study it was necessary to bring the model into a state that could be called at least "close-to-steady state." More than 20,000 model years were necessary for this integration. Owing to the chosen spatial resolution, the distribution of silicic acid reflects the broad pattern very well, but loses accuracy in the small-scale details. For instance, regional upwelling along the Peruvian coast and winter convection around the Antarctic peninsula are either under- or over-represented in the model. The question now is, to what extent do the model drawbacks influence the results, i.e., the distribution of δ^{30}Si, especially in the surface and the sediment of the Southern Ocean and the equatorial Pacific?

[49] There is still a uniformly drift of the deep ocean δ^{30}Si$_{DSi}$. In equilibrium the global deep ocean average will be about 0.18‰ higher than it is after integrating 23,000 model years. This will lead to a maximum increase of the upwelled δ^{30}Si$_{DSi}$ of 0.18‰ and will shift all signals toward higher δ^{30}Si. Given the range of the δ^{30}Si signals found in the surface and the sediment, this will not make a big change to the conclusions drawn before, but rather shifts the calculated sediment values closer to the few measured ones.

[50] As was shown in the literature, the current system of the equatorial Pacific is very complex, with its meridional overturning cells and the transport of nutrients in the area between 2.5°S to 2.5°N [e.g., *Johnson et al.*, 1999]. In HAMOCC4 this latitudinal range is represented by two grid boxes and therefore does not show the small details in silicic acid concentrations found, for example, in the World Ocean Atlas [*Conkright et al.*, 1998]. Still, the HAMOCC4 is capable of reproducing the most important feature for the silicic acid supply to the system, which is the Equatorial Undercurrent, with about the correct size of upwelling (52 Sv in the area 170°W−95°W, 3.6°S−5.2°N compared to 62 ± 18 Sv from geostrophic calculations by *Johnson and McPhaden* [2001]). Bearing in mind that the upwelling at the Peruvian coast might be under-represented and that the model resolution is 3.5° × 3.5°, the relation between δ^{30}Si$_{opal}$ in the sediment and the silicic acid surface concentration should be generally valid in the open ocean area, but might be not as smooth as shown by the model. In the eastern equatorial Pacific, simulated surface silicic acid concentrations are possibly higher than measured. Either model productivity in this area is too low or vertical transport of nutrients is too pronounced despite the correct size of upwelling. Generally, δ^{30}Si$_{opal}$ increases with decreasing silicic acid concentrations. The model may thus underestimate the amplitude of the signal in the eastern equatorial Pacific sediment.

[51] Furthermore, the missing iron limitation of diatom growth may lead to different patterns of opal and silicic acid. This is of interest in the North Pacific and the Southern Ocean. Since the LSG dynamics seem to overestimate

stratification or underestimate vertical nutrient transport in the North Pacific [*Aumont et al.*, 2003], we do not rely on the δ^{30}Si signal there. Differences in modeled and measured silicic acid concentrations are largest in the Southern Ocean with its very high silicic acid concentrations. Since concentrations are still high enough to keep the silicic acid depletion low, the error in the δ^{30}Si signal might be small.

[52] Silicic acid limitation of diatom growth is reported for the area north of the Southern Ocean Polar Front [*Boyd et al.*, 2000], which would lead to high δ^{30}Si$_{opal}$. This feature is not very well simulated in the model, possibly because the large diatom blooms found at the Polar Front cannot be represented locally. Hence the strongest δ^{30}Si$_{opal}$ signal is found farther north. This may be another reason to expect higher isotope compositions in the sediments directly north of the Polar Front.

6. Conclusions

[53] For the first time, the overall distribution of silicon isotopes in the world ocean has been calculated by integration of a biogeochemical ocean circulation model. It has been shown that the relationship between the silicic acid concentration in the water and its silicon isotope composition, δ^{30}Si$_{DSi}$, is not a simple Rayleigh distillation curve. Only the Southern Ocean and the equatorial Pacific show a clear functional dependency similar to the Rayleigh distillation curve. The model results can be used to predict opal silicon isotope compositions in the sediment. The accumulated opal isotope signal is much more variable than the signal of the dissolved phase. More importantly, the model results can be used to further constrain the use of silicon isotopes as a proxy for silicic acid utilization. Owing to the nature of the Pacific current system, it might be valid to even apply a relationship between silicic acid concentrations in the surface and the silicon isotope signal in the sediment. This should be further confirmed by silicon isotope measurements and the incorporation of silicon isotopes in higher-resolution models. Generally, more opal isotope data is needed to further examine the use of this promising proxy.

References

Arakawa, A., and V. R. Lamb, Computational design of the basic dynamical process of the UCLA general circulation model, *Methods Comput. Phys.*, *16*, 173−283, 1977.

Aumont, O., E. Maier-Reimer, S. Blain, and P. Monfray, An ecosystem model of the global ocean including Fe, Si, P co-limitations, *Global Biogeochem. Cycles*, *17*, 1060, doi:10.1029/2001GB001745, 2003.

Boyd, P. W., et al., A mesoscale phytoplankton bloom in the polar Southern Ocean stimulated by iron fertilization, *Nature*, *407*, 695−702, 2000.

Brzezinski, M. A., C. J. Pride, V. M. Franck, D. M. Sigman, J. L. Sarmiento, K. Matsumoto, N. Gruber, G. H. Rau, and K. H. Coale, A switch from Si(OH)4 to NO3- depletion in the glacial Southern Ocean, *Geophys. Res. Lett.*, *29*(12), 1564, doi:10.1029/2001GL014349, 2002.

Conkright, M., S. Levitus, T. O'Brien, T. Boyer, J. Antonov, and C. Stephens, *World Ocean Atlas 1998 CD-ROM Data Set Documentation*, *Tech. Rep. 15*, pp. 1−16, Natl. Oceanic and Atmos. Admin., Silver Spring, Md., 1998.

Coplen, T. B., et al., Compilation of minimum and maximum isotope ratios of selected elements in naturally occurring terrestrial materials and re-

agents, *Water Resour. Invest. Rep. 01-4222*, 98 pp., U.S. Geol. Surv., U.S. Dep. of Interior, Washington, D. C., 2002.

Criss, R. E., *Principles of Stable Isotope Distribution*, Oxford Univ. Press, New York, 1999.

De La Rocha, C. L., Silicon isotope fractionation by marine sponges and the reconstruction of the silicon isotope composition of ancient deepwater, *Geology*, *31*(5), 423–426, 2003.

De La Rocha, C. L., M. A. Brzezinski, and M. J. DeNiro, Fractionation of silicon isotopes by marine diatoms during biogenic silica formation, *Geochim. Cosmochim. Acta*, *61*, 5051–5056, 1997.

De La Rocha, C. L., M. A. Brzezinski, M. J. DeNiro, and A. Shemesh, Silicon-isotope composition of diatoms as an indicator of past oceanic change, *Nature*, *395*, 680–683, 1998.

De La Rocha, C. L., M. A. Brzezinski, and M. J. DeNiro, A first look at the distribution of the stable isotopes of silicon in natural waters, *Geochim. Cosmochim. Acta*, *64*, 2467–2477, 2000.

Dutay, J.-C., et al., Evaluation of ocean model ventilation with CFC-11: Comparison of 13 global ocean models, *Ocean Modell.*, *4*(2), 89–120, 2002.

Eppley, R. W., Temperature and phytoplankton growth in the sea, *Fish. Bull.*, *70*, 1063–1085, 1972.

Heinze, C., E. Maier-Reimer, A. M. E. Winguth, and D. Archer, A global oceanic sediment model for long-term climate studies, *Global Biogeochem. Cycles*, *13*, 221–250, 1999.

Hellerman, S., and M. Rosenstein, Normal monthly wind stress over the world ocean with error estimates, *J. Phys. Oceanogr.*, *13*, 1093–1104, 1983.

Johnson, G. C., and M. McPhaden, Equatorial Pacific Ocean horizontal velocity, divergence, and upwelling, *J. Phys. Oceanogr.*, *31*, 839–849, 2001.

Johnson, K. S., F. P. Chavez, and G. E. Friederich, Continental-shelf sediment as a primary source of iron for coastal phytoplankton, *Nature*, *398*, 697–700, 1999.

Kamatami, A., and J. P. Riley, Rate of dissolution of diatom silica walls in seawater, *Mar. Biol.*, *68*, 91–96, 1979.

Levitus, S., (Ed.), Climatological atlas of the world ocean, *NOAA Prof. Pap.13*, 173 pp., U.S. Govt. Print. Off., Washington, D. C., 1982.

Loubere, P., Marine control of biological production in the eastern equatorial Pacific Ocean, *Nature*, *406*, 497–500, 2000.

Maier-Reimer, E., Geochemical cycles in an ocean general dirculation model: Preindustrial tracer distributions, *Global Biogeochem. Cycles*, *7*, 645–677, 1993.

Maier-Reimer, E., U. Mikolajewicz, and K. Hasselmann, Mean circulation of the Hamburg LSG OGCM and its sensitivity to the thermohaline surface forcing, *J. Phys. Oceanogr.*, *23*, 731–757, 1993.

Martin, J. H., and S. E. Fitzwater, Iron deficiency limits phytoplankton growth in the northeast Pacific subarctic, *Nature*, *331*, 341–343, 1988.

Nelson, D. M., et al., Vertical budgets for organic carbon and biogenic silica in the Pacific ector of the Southern Ocean, 1996–1998, *Deep Sea Res., Part II*, *49*, 1645–1674, 2002.

Pondaven, P., O. Ragueneau, P. Tréguer, A. Hauvespre, L. Dezileau, and J. L. Reyss, Resolving the 'opal paradox' in the Southern Ocean, *Nature*, *405*, 168–172, 2000.

Ragueneau, O., et al., A review of the Si cycle in the modern ocean: Recent progress and missing gaps in the application of biogenic opal as a paleoproductivity proxy, *Global Planet. Change*, *26*, 317–365, 2000.

Rosman, K. J. R., and P. D. P. Taylor, Isotopic compositions of the elements: Technical report, *Pure Appl. Chem.*, *70*(1), 217–235, 1998.

Six, K. D., and E. Maier-Reimer, Effects of plankton dynamics on seasonal carbon fluxes in an ocean general circulation model, *Global Biogeochem. Cycles*, *10*, 559–583, 1996.

Sloyan, B. M., and S. R. Rintoul, The Southern Ocean Limb of the Global Deep Overturning Circulation, *J. Phys. Oceanogr.*, *31*, 143–173, 2001.

Smith, L. E., Photosynthesis in relation to light and carbon dioxide, *Proc. Natl. Acad. Sci. U. S. A.*, *22*, 504–511, 1936.

Spadaro, P. A., Silicon isotope fractionation by the marine diatom Phaeodactylum tricornutum, Master's thesis, Univ. of Chicago, Chicago, Ill., 1983.

Tréguer, P., A. Kamatami, S. Gueneley, and B. Quéguiner, Kinetics of dissolution of Antarctic diatom frustules and the biogeochemical cycle of silicon in the Southern Ocean, *Polar Biol.*, *9*, 397–403, 1989.

Tréguer, P., D. M. Nelson, A. J. van Bennekom, D. J. DeMaster, A. Leynaert, and B. Quéguiner, The silica balance in the world ocean: A reestimate, *Science*, *268*, 375–379, 1995.

Varela, D. E., C. J. Pride, M. A. Brzezinski, and M. J. DeNiro, Natural variations in silicon isotope abundances as indicators of silica production in the Southern Ocean, *Eos Trans, AGU*, *83*(4), Ocean Sci. Meet. Suppl., OS21L–08, 2002.

Wefer, G., W. H. Berger, J. Bijma, and G. Fischer, Clues to ocean history: A brief overview of proxies, in *Use of Proxies in Paleoceanography*, edited by G. Fischer and G. Wefer, pp. 1–68, Springer-Verlag, New York, 1999.

Woodruff, S. D., et al., A comprehensive ocean-atmosphere data set, *Bull. Am. Meteorol. Soc.*, *68*, 1239–1250, 1987.

————————————

C. L. De La Rocha, Department of Earth Sciences, University of Cambridge, Downing Street, Cambridge, CB2 3EQ, UK. (christina00@esc.cam.ac.uk)

E. Maier-Reimer, Max Planck Institute for Meteorology, Bundesstrasse 55, D-20146 Hamburg, Germany. (maier-reimer@dkrz.de)

A. G. Wischmeyer and D. A. Wolf-Gladrow, Alfred Wegener Institute for Polar and Marine Research, Am Handelshafen 12, D-27570 Bremerhaven, Germany. (wolf@awi-bremerhaven.de; awischmeyer@awi-bremerhaven.de)